PACS numbers: 42.65.Dr; 42.62.Fi
DOI: 10.1070/QE2002v032n01ABEH002123

Manifestations of collisions in the laser SRS–CARS diagnostics of hydrogen in rarefied gas mixtures

Gen.M.Mikheev, Geor.M.Mikheev, T.N.Mogileva, D.G.Kalyuzhnyi

***Abstract*. CARS diagnostics of hydrogen in rarefied gas mixtures is performed using the biharmonic laser pump based on the SRS by the vibrational hydrogen transition. The diagnostics is shown to be substantially affected by collisions, which result in variations in the linewidth and the frequency of the Raman-active transition. This influence is distinctly observed at pressures higher than 0.05 atm and depends on the composition of the buffer gas mixture.**

Keywords: *stimulated Raman scattering, coherent anti-Stokes Raman spectroscopy, line shift and broadening, gas mixtures.*

1. Introduction

The development of the methods for hydrogen diagnostics in matter based on the advances of quantum electronics is of interest both for scientific studies and for practical applications. When studying the effect of hydrogen on the properties of metal alloys, many researchers estimate its content in the samples only indirectly, for instance, by time and current (in the case of electrolytic hydrogen adsorption [1]), or by using high-vacuum mass spectrometers [2]. In addition, it is often necessary to analyse rapidly the hydrogen content in dielectric liquids for detecting the electric and thermal damages in high-voltage oil-filled systems. This stimulates the further development of the well-known CARS technique involving SRS [3] for laser diagnostics of hydrogen in gas mixtures. The aim of our work is to study the effect of buffer gas pressure on the SRS–CARS signal at a constant hydrogen density in rarefied gas mixtures.

2. Specific features of SRS–CARS diagnostics of hydrogen

CARS is a four-photon parametric process in which the mixing of two laser beams with frequencies ω_p and ω_s in a medium possessing a cubic nonlinear susceptibility $\chi^{(3)}$ results in the generation of coherent directional radiation at the anti-Stokes frequency $\omega_a = 2\omega_p - \omega_s$ [4]. The principle of this method, as applied to the diagnostics of H_2 in a gas mixture, is the following. The medium is probed by a biharmonic laser pump (BLP) at frequencies ω_p and ω_s which satisfy the condition of approximate resonance:

$$\omega_p - \omega_s \approx \Omega_\rho, \tag{1}$$

where Ω_ρ is the frequency of the $Q_{01}(1)$ Raman transition of hydrogen mixed with gas at a density ρ (Fig. 1). In this case, the intensity of radiation I_a at the frequency ω_a is

$$I_a \sim \left|\chi_r^{(3)} + \chi_{nr}^{(3)}\right|^2 I_p^2 I_s, \tag{2}$$

where I_p and I_s are the intensities of radiation at the frequencies ω_p and ω_s; $\chi_r^{(3)}$ is the cubic resonance susceptibility of the molecules of the gas under study; $\chi_{nr}^{(3)} = n_{bg}\gamma_{nr}$ is the cubic nonresonance susceptibility due to the electron contribution and related primarily to the participation of buffer gas molecules in a scattering event; $\chi_r^{(3)} = n_{H_2}\gamma_r$; γ_r and γ_{nr} are the cubic hyperpolarisabilities of the gas under study and the buffer gas, respectively; and n_{H_2} and n_{bg} are the number densities of the hydrogen and buffer gas molecules.

The cubic resonance susceptibility $\chi_r^{(3)}$ is defined by the expression [5]:

$$\chi_r^{(3)} = \frac{1}{3}\Delta_k^n \frac{2\pi n_{H_2} c^4}{h\Gamma\omega_s^4}\frac{d\sigma}{do}\frac{\Gamma}{\Omega_\rho - (\omega_p - \omega_s) - i\Gamma}, \tag{3}$$

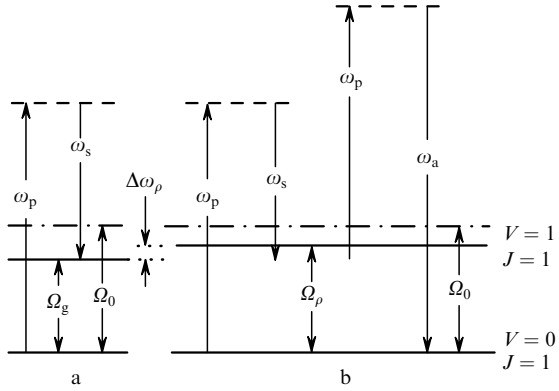

Figure 1. Energy level diagram of the $Q_{01}(1)$ vibrational transition of hydrogen in an SRS oscillator (a) and in a rarefied gas mixture (b), and also diagrams illustrating SRS (a) and CARS (b) methods.

Gen.M.Mikheev, T.N.Mogileva, D.G.Kalyuzhnyi Institute of Applied Mechanics, Ural Division, Russian Academy of Sciences, ul. M.Gor'kogo 222, 426000 Izhevsk, Russia; e-mail: mikheev@udmnet.ru
Geor.M.Mikheev 'Chuvashenergo' Joint Stock Co., prosp. Lenina 40, 428000 Cheboksary, Russia

Received 7 July 2001; revision received 4 December 2001.
Kvantovaya Elektronika **32** (1) 39–44 (2002)
Translated by E.N.Ragozin

where Γ is the line half-width at half maximum (HWHM) for a Raman-active transition; Δ_k^n is the difference of level populations; $d\sigma/do$ is the molecular cross section for spontaneous Raman scattering by the above transition. It follows from expression (3) that $|\chi_r^{(3)}|$ significantly decreases for $|\Omega_\rho - (\omega_p - \omega_s)| \gg \Gamma$. This means that under the condition (1), I_a is primarily determined by the scattering by the impurity molecules to be detected.

Consider the problem of measuring the hydrogen concentration n_{H_2} by the CARS method in low-density gas mixtures satisfying the condition

$$\rho \ll 1 \text{ amagat}, \tag{4}$$

where ρ is the density of the gas mixture [18]. In this case, when the condition (1) is fulfilled it is possible to neglect the contribution of $\chi_{nr}^{(3)}$ in expression (2) and write (2) in the form:

$$\left(\frac{I_a}{I_p^2 I_s}\right)^{1/2} = \frac{b_a n_{H_2}}{\left[\Gamma_\rho^2 + \Delta\omega_\rho^2\right]^{1/2}}, \tag{5}$$

where b_a is the proportionality coefficient; Γ_ρ is the line HWHM of the H_2 transition for a buffer gas density ρ; and $\Delta\omega_\rho = (\omega_p - \omega_s) - \Omega_\rho = \Omega_g - \Omega_\rho$ (Fig. 1).

From (5), we obtain the expression for n_{H_2}:

$$n_{H_2} = \frac{1}{b_a}\left(\frac{I_a}{I_p^2 I_s}\right)^{1/2}\left(\Gamma_\rho^2 + \Delta\omega_\rho^2\right)^{1/2}. \tag{6}$$

In low-density gas mixtures subject to the condition (4), the line HWHM Γ_ρ is determined only by Doppler broadening, which depends on the temperature T [6]. Therefore, for constant T and $\Delta\omega_\rho$ under the condition (4), the concentration n_{H_2} can be determined by measuring the intensity of radiation at the frequencies ω_a, ω_p, and ω_s. A BLP simultaneously satisfying the conditions (1) and $\Delta\omega_\rho = \text{const}$ can be obtained by SRS in compressed hydrogen, for instance, by the $Q_{01}(1)$ vibrational transition (Fig. 1a) [3, 7–9]. In this case, the laser part of the setup becomes significantly simpler.

Consider now the case when the gas mixture density satisfies the condition

$$\rho \leqslant 1 \text{ amagat}, \tag{7}$$

In this case, upon the detection of very low (background) hydrogen concentrations, the contribution of the nonresonance susceptibility $\chi_{nr}^{(3)}$ to the CARS signal may be significant. One way of reducing this nonresonance background in the stationary CARS spectroscopy involves employing a complex polarisation technique [4]. In no less complex technique of transient (picosecond) CARS spectroscopy, the nonresonance signal is automatically eliminated owing to the difference in dephasing times of molecular vibrations and the electronic nonlinearity [10, 11].

However, there is no need to use such sophisticated methods in many cases when the concentration of H_2 is much higher than the background concentration because experiments show that the nonresonance background is manifested only when $n_{H_2}/n_{bg} < 10^{-5}$. This means that expressions (5) and (6) can be also used in the SRS–CARS diagnostics of gas mixtures that satisfy the condition (7) and contain hydrogen at concentrations significantly higher than the background one. However, the SRS–CARS signal measured in this case can significantly and nonlinearly depend on the total density ρ. Consider this property, which was not observed in earlier papers [3, 7–9, 12] in the SRS–CARS diagnostics of gas mixtures.

3. Effect of collisions on the SRS–CARS signal

It is well known that the frequency and linewidth of the $Q_{01}(1)$ Raman transition in a hydrogen molecule depend on the gas pressure [13, 14]. They also depend on the pressure of a buffer gas (see, for instance, Ref. [15]). For pure H_2 at room temperature, the $Q_{01}(1)$ linewidth begins to vary even at pressures above 0.2 atm [6]. Therefore, when low concentrations of H_2 are measured in a gas mixture at about an atmospheric total pressure, the SRS–CARS signal may depend on the density of the gas mixture even at a constant concentration of hydrogen. This may be caused by two mechanisms – the collisional Dicke narrowing and a change in the H_2 Raman transition frequency with increasing the total pressure of the gas mixture [13, 16–18] – which are responsible for the variations in Γ_ρ and $\Delta\omega_\rho$ in expression (5).

The Doppler effect is known to be one of the main causes of spectral line broadening. However, any factor that limits or decelerates the motion of oscillators should result in the narrowing of the Doppler line profile $\Delta\omega_D$ [16]. For this reason, the collisions that increase the average time requires for the shift of particles by a distance of the order of the radiation wavelength cause the narrowing of the emission spectrum compared to $\Delta\omega_D$.

This effect is especially significant when the relation $l \ll 1/k_e$ is fulfilled, where l is the particle mean free path and k_e is the effective wavenumber. The physical essence of the Dicke narrowing effect consists in that the collisions of particles in a medium having the phase memory do not result in the collisional line broadening, but limit the motion of particles, thereby eliminating the inhomogeneous Doppler broadening. Therefore, with increasing gas density, the Doppler width decreases to attain a certain minimum (the Dicke narrowing). Then the linewidth increases linearly with the gas density due to collisional broadening.

These features were experimentally observed in pure H_2 in the studies of the linewidths of vibrational [17–20] and rotational [21, 22] Raman transitions. The Dicke narrowing was demonstrated at rather high concentrations of hydrogen mixed with CH_4 [23], He, and Ar [24]. The line broadening of the rotational transitions of H_2 and D_2 in different (He, Ar, O_2, N_2, CO, HCl) high-pressure mixtures was investigated in Ref. [25]. The frequency shift of the vibrational transition of hydrogen in gas mixtures with increasing pressure was investigated in Refs [26–28].

According to the diffusion model, which describes the collisional Dicke narrowing, the line HWHM Γ_ρ for pure gas is described by the expression [6, 29]:

$$\Gamma_\rho = \frac{A}{\rho} + B\rho, \tag{8}$$

where $A = 4\pi^2 D_0/\lambda^2$; D_0 is the gas diffusion coefficient under normal conditions; λ is the radiation wavelength of the transition under study; and B is the collisional broadening coefficient for Γ_ρ. Note that this formula is invalid for $\rho \to 0$. Nevertheless, it follows from (8) that the linewidth is minimal for the optimal gas density

$$\rho_{\text{opt}} = \left(\frac{A}{B}\right)^{1/2}. \quad (9)$$

For the forward spontaneous Raman scattering by the $Q_{01}(1)$ vibrational transition in H_2 at 298 K ($D_{0\,H_2-H_2} = 1.35$ cm^2 amagat s^{-1}, $B = 8.4 \times 10^{-4}$ cm^{-1} amagat^{-1} [19]), the calculated optimal density is 2.5 amagat, which agrees well with the experimentally determined value of ρ_{opt} [6].

It is evident that the half-width of the $Q_{01}(1)$ transition line of hydrogen molecules mixed with a buffer gas is described by the same expression (8) with increasing buffer gas density. However, one should keep in mind that the diffusion coefficient for hydrogen, for instance, in carbon dioxide is several times lower and, according to Ref. [30], is only 0.58 cm^2 amagat s^{-1}. In addition, the heavier the buffer gas particles, the greater the collisional broadening coefficient B [26, 28]. This all has the effect that the Dicke narrowing in hydrogen–buffer gas mixtures will manifest itself with increasing buffer gas density for lower ρ than for pure hydrogen. Therefore, the SRS–CARS signal in rarefied gas mixtures will depend on the composition and pressure of the buffer gas at a constant concentration of hydrogen in the measuring cell. In addition, the SRS–CARS signal determined by formula (5) will vary with decreasing or increasing the frequency detuning $\Delta\omega_\rho$, caused by collisions and dependent on the density ρ and the composition of the buffer gas:

$$\Delta\omega_\rho = \Delta\omega_0 - \alpha_{\text{bg}}\rho - \beta_{\text{bg}}\rho^2, \quad (10)$$

where

$$\Delta\omega_0 = \Omega_{\text{g}} - \Omega_0 = \alpha_{H_2}\rho_{H_2} + \beta_{H_2}\rho_{H_2}^2; \quad (11)$$

Ω_0 and Ω_{g} are the frequencies of the Raman-active hydrogen transition for a zero density and in the SRS oscillator, respectively; α_{H_2}, β_{H_2} and α_{bg}, β_{bg} are the coefficients that determine the shift of the transition frequency Ω_0 with increasing density in pure hydrogen and in hydrogen mixed with the buffer gas, respectively; and ρ_{H_2} is the hydrogen density in the SRS oscillator.

Note that the CARS signal in the measuring cell can also depend on the phase mismatch of the interacting waves caused by a change in the coherent interaction length l_{coh} upon variations in the buffer gas density. According to Ref. [4], for parallel beams, the length l_{coh} is inversely proportional to the wave detuning Δk: $l_{\text{coh}} = \pi/\Delta k$, where $\Delta k = k_{\text{a}} - 2k_{\text{p}} + k_{\text{s}}$; k_{p}, k_{s}, and k_{a} are the respective wavenumbers of the frequency components ω_{p}, ω_{s}, and ω_{a}, respectively.

It is well known that Δk is proportional to $\rho^{1/2}$. Estimates show that the coherent interaction length for an atmospheric pressure of the buffer gas, for instance, argon, amounts to several tens of centimetres, which is far greater than the interaction length of focused beams. Therefore, the CARS signal variation in rarefied gas mixtures ($\rho < 1$ amagat) caused by the phase mismatch of the interacting waves due to variations in the buffer gas density will not be observed.

4. Experimental

The simplified optical scheme of the experiment is shown in Fig. 2. The pump generator (*1*) was a single-mode Nd^{3+}:YAG laser with a passive F_2^-:LiF-crystal based Q-switching and a frequency conversion to the second harmonic employing a KTP crystal [31]. The peak energy of a 532-nm pulse was 40 mJ, the pulse duration was $\tau_{\text{p}} = 7$ ns, and the divergence was about 0.6 mrad. The output laser radiation was focused with a deflecting mirror (*2*) and a lens (*3*) ($F_1 = 0.66$ m) in an SRS cell (*4*) ($L_1 = 0.86$ m) with compressed molecular hydrogen at a density of 2.8 amagat. The BLP generated in the cell (*4*) due to the SRS by the $Q_{01}(1)$ vibrational transition was collimated by a lens (*5*), separated from other SRS components with a filter set (*6*), and focused in a measuring cell (*10*) ($L_2 = 0.21$ m) with an objective lens (*9*) ($F_2 = 0.1$ m). The anti-Stokes component excited in the cell (*10*) due to CARS was directed to the entrance slit of a monochromator (*13*) with the help of a lens (*11*) and a prism (*12*).

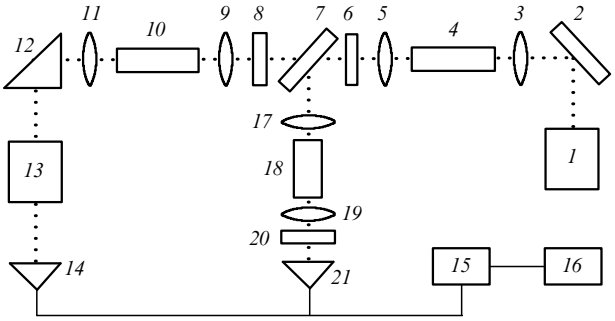

Figure 2. Scheme of the experiment.

The signal was detected with a photomultiplier (*14*) and a multichannel system for recording the energy of laser pulses (*15*) coupled to a microcomputer (*16*). A part of the BLP after a beamsplitter (*7*) was focused by a lens (*17*) at the centre of a reference cell (*18*) with a fixed density of 2.8 amagat. The anti-Stokes scattering component produced in the reference cell (*18*) was directed to the photodiode (*21*) with a lens (*19*), through a filter set (*20*). This additional optical branch containing elements (*17–21*) made it possible to normalise the signal originating in the measuring cell (*10*) and eliminate the effect of intensity fluctuations of the exciting SRS laser.

Note that the use of the reference optical branch (*17–21*) allowed us to measure the SRS–CARS signal in the measuring cell, proportional to $(I_{\text{a}}/I_{\text{p}}^2 I_{\text{s}})^{1/2}$, without the corresponding measurement of BLP component intensities. To eliminate the possible saturation effect [8], which is responsible for the spectral shape distortion of the CARS signal, the intensity of biharmonic pump at the input of the measuring cell was attenuated employing neutral density filters (*8*).

Prior to experiments, the air was evacuated from the measuring cell down to about 0.1 kPa. After that, a portion of hydrogen was admitted to cell to provide a density of $\sim 4 \times 10^{-3}$ amagat. A buffer gas was next admitted to the same cell; as the buffer gas, we used air, helium, argon, oxygen, nitrogen, carbon dioxide, ethane, and propane. No care was taken to purify these gases from possible H_2 impurity content. The pressure of the above gases in the measuring cell was smoothly raised with a special bleed-in system. In this case, measurements were performed no less than 15 minutes after the admission of each portion of the buffer gas. The hydrogen contained in the measuring cell

and the buffer gas admitted to the cell managed to get evenly mixed up during this time period. All experiments were performed at room temperature, which was taken into account in the density calculation of the gas mixture in the measuring cell.

5. Experimental results and discussion

Fig. 3 shows experimental dependences, which illustrate the effect of propane gas density on the SRS–CARS signal. The experimental dependence (*1*) was obtained under the following conditions: the propane gas was gradually admitted to the measuring cell, from which the air had been evacuated to a pressure of less than 0.1 kPa, up to atmospheric pressure. Curve (*1*) in Fig. 3a shows that the increase in the propane pressure up to the atmospheric one in the absence of hydrogen results in only an insignificant increase of the signal.

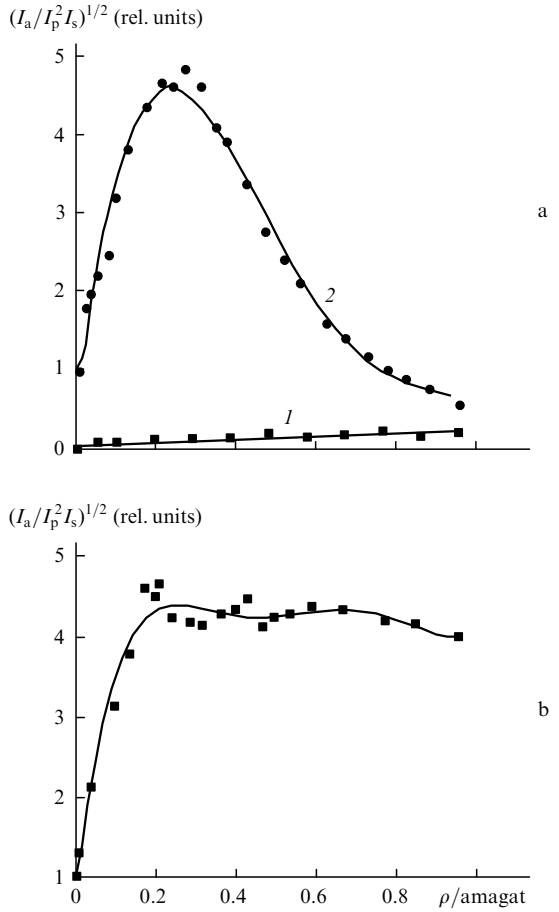

Figure 3. Normalised signal $(I_a/I_p^2I_s)^{1/2}$, measured for a zero (*1*) and some fixed (*2*) concentration of hydrogen in the measuring cell, as functions of the propane (a) and propane–helium mixture (b) buffer-gas density ρ (propane for $\rho < 0.2$ amagat; 0.2 amagat of propane + helium for $\rho > 0.2$ amagat).

The experimental curve (*2*) in Fig. 3a was obtained under the same conditions, with the only difference that after the air evacuation a portion of molecular hydrogen was admitted to the measuring cell to provide a pressure of 0.4 kPa. In this case, a rather intense signal appeared at once in the measuring cell (*10*), whose intensity was taken as unity. Then, propane was gradually admitted to the measuring cell (see above). One can see that increasing the propane density in the cell results in a significant signal growth. The SRS–CARS signal reaches a maximum at some optimal propane buffer gas density $\rho_{opt}(C_3H_8) \approx 0.2 - 0.25$ amagat and then monotonically desreases with increasing ρ.

We performed similar investigations with other gases, such as, He, Ar, Co_2, C_2H_6, O_2, and air. The results of these experiments are shown in Fig. 4. Note that the dependences $(I_a/I_p^2I_s)^{1/2}(\rho)$ obtained for these gases without the admission of hydrogen ($\rho_{H_2} = 0$) are nearly coincident with the abscissa axis and are therefore not shown.

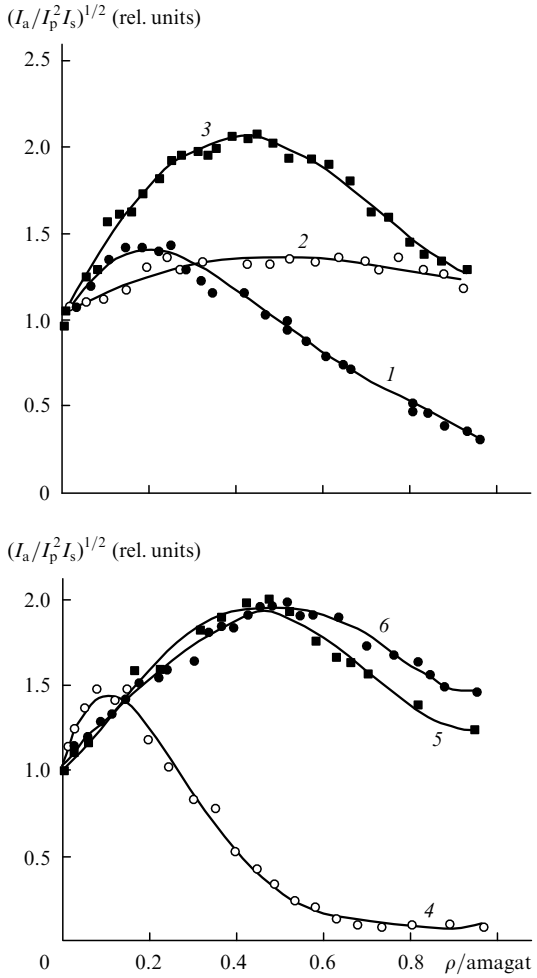

Figure 4. Normalised signal $(I_a/I_p^2I_s)^{1/2}$, measured for a fixed concentration of hydrogen in the measuring cell, as functions of the density ρ of different buffer gases: carbon dioxide (*1*), helium (*2*), argon (*3*), ethane (*4*), oxygen (*5*), and air (*6*).

It is interesting that the experimental dependences presented in Figs 3a and 4 are similar in character. The signal first increases with increasing buffer gas density, then reaches a maximum, and the quantity $(I_a/I_p^2I_s)^{1/2}$ being measured tends to become lower as ρ is further increased. At the same time, these dependences significantly differ from one another by the peak amplitude and the gas density ρ_{opt} at which this peak is observed.

Among the gases considered, helium has the weakest effect on the signal (Fig. 4, curve *2*), while propane has the

strongest effect (Fig. 3a, curve *2*). For argon, $\rho_{opt}(Ar) = 0.4$ amagat (Fig. 4, curve *3*). For carbon dioxide, $\rho_{opt}(CO_2) = 0.2$ amagat (Fig. 4, curve *1*). The dependences $[I_a \times (I_p^2 I_s)^{-1}]^{1/2}(\rho)$ obtained for air (Fig. 4, curve 6) and oxygen (Fig. 4, curve 5) are most close to each other. Furthermore, the experimental dependences $(I_a/I_p^2 I_s)^{1/2}(\rho)$ obtained for different gases for a fixed hydrogen concentration differ from one another for $\rho \approx 1$ amagat. Indeed, for an atmospheric pressure of carbon dioxide (Fig. 4, curve *1*), propane (Fig. 3a, curve *2*), and ethane (Fig. 4, curve *4*), the normalised SRS–CARS signal is significantly lower than unity. At the same time, for the gas mixtures of hydrogen with air, oxygen, helium, and argon it remains greater than unity.

Of some interest is obtaining a high SRS–CARS signal at atmospheric pressure. An analysis of the dependences shown in Fig. 3a (curve *2*) and Fig. 4 (curve *2*) suggests that the use of propane up to densities of 0.2–0.25 amagat will permit obtaining a high signal. This signal may be also retained for higher densities of the gas mixture produced through the addition of helium, which has only a weak effect on the signal. This is confirmed by the experimental curve plotted in Fig. 3b. It was obtained under the same conditions as curve *2* in Fig. 3a. The only difference was that the increase in gas density, subsequent to the admission of 0.2 amagat of propane to the measuring cell, was accomplished through the addition of helium. In this case, as is evident from Fig. 3, the high SRS–CARS signal is virtually retained up to the atmospheric pressure. This all is indication that the SRS–CARS signal may depend significantly not only on the density and kind of the buffer gas, but also on its components.

The experimental data presented in Figs 3 and 4 are in qualitative agreement with expressions (5), (8), and (10). Indeed, according to expression (5), the experimental dependence obtained, for instance, for the H_2–Ar gas mixture (Fig. 4, curve *3*) can be represented in a different X, Y coordinate system, where

$$X = \rho;\ Y = k = \frac{\left(I_a/I_p^2 I_s\right)_{\rho=0}^{1/2}}{\left(I_a/I_p^2 I_s\right)_{\rho}^{1/2}} = \left(\frac{\Gamma_\rho^2 + \Delta\omega_\rho^2}{\Delta\omega_D^2 + \Delta\omega_0^2}\right)^{1/2}; \quad (12)$$

Γ_ρ and $\Delta\omega_\rho$ are the line HWHM and the frequency detuning for an argon density ρ (Fig. 5).

Then, we determine three fitting coefficients for the calculated $k(\rho)$ curve. To this end, for simplicity we assume that the line HWHM Γ_ρ is expressed in terms of ρ by the formula (8) and in doing this we neglect the experimental data obtained for $\rho < 0.3$ amagat. Furthermore, we take into account only the first two terms in expression (10) for $\Delta\omega_\rho$. For $T = 298$ K we determine $\Delta\omega_D$ (18.15×10^{-3} cm^{-1}) and from the data of Ref. [6] we calculate $\Delta\omega_0$ (-8.9×10^{-3} cm^{-1}) that corresponds to the gas density in the SRS oscillator for $\rho_{H_2} = 2.8$ amagat. As a result, we find the diffusion coefficient D_{H_2-Ar}, the collisional broadening coefficient for the B_{H_2-Ar} line HWHM, and also the linear coefficient for the frequency shift of the α_{H_2-Ar} Raman transition of hydrogen in argon, which were equal to 0.53 cm^2 amagat s^{-1}, 12.3×10^{-3} cm^{-1} amagat^{-1}, and -18.5×10^{-3} cm^{-1} amagat^{-1}, respectively. The obtained coefficients D_{H_2-Ar}, B_{H_2-Ar}, and α_{H_2-Ar} by the order of magnitude agree with those obtained in Refs [24, 25], which are equal to 0.8 cm^2 amagat s^{-1}, 4.42×10^{-3} cm^{-1} amagat^{-1}, and -11.82×10^{-3} cm^{-1} amagat^{-1}, respectively. It is conceivable that a more precise determination of the above coefficients from our data would require not the simple formula of the diffusion model (8) but the use of the strong-collision model [6, 16], which provides a better description of the dependence $\Gamma_\rho(\rho)$ at low gas densities.

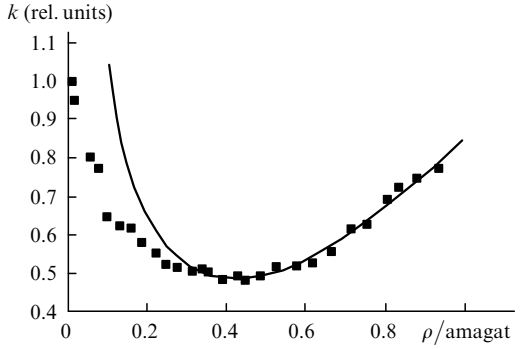

Figure 5. Experimental dependence of the normalised coefficient k on the argon density ρ (squares) and fitting curve $k(\rho)$ (solid line).

6. Conclusions

Therefore, the results outlined above lead to the conclusion that the SRS–CARS signal may be substantially dependent on the composition and density of the buffer gas for a fixed concentration of hydrogen in a rarefied gas mixture in the presenceof a weak nonresonance background. This was experimentally shown by the example of He, Ar, CO_2, O_2, air, C_2H_6, and C_3H_8. This dependence is due to the effect of collisions on the linewidth and frequency shift of the Raman-active transition of hydrogen and is clearly manifested at pressures above 0.05 atm.

Acknowledgements. This work was supported by the Russian Foundation for Basic Research (Grant No. 01-02-96461).

References

1. Spivak L.V., Khonik V.A., Skryabina N.E. *Pis'ma Zh. Tekh. Fiz.*, **19** (7), 40 (1993).
2. Zaluzhnyi A.G., Kalin B.A., Kopytin V.P., Kozodaev M.A., Suvorov A.L. *Zh. Tekh. Fiz.*, **71**, 31 (2001) [*J. Tech. Phys.*, **46**, 29 (2001)].
3. Regnier P.R., Taran J.P.E. *Appl. Phys. Lett.*, **23**, 240 (1973).
4. Akhmanov S.A., Koroteev N.I. *Metody nelineinoi optiki v spektroskopii rasseyaniya sveta* (Methods of Nonlinear Optics in Light Scattering Spectroscopy) (Moscow: Nauka, 1981).
5. Bunkin A.F., Ivanov S.G. *Kvantovaya Elektron*, **9**, 1821 (1982) [*Sov. J. Quantum Electron.*, **12**, 1172 (1982)].
6. Bischel W.K., Dyer M.J. *Phys. Rev. A*, **33**, 3113 (1986).
7. Ivanov A.A., Polyakov G.A., Voronin V.B. *Izv. Akad. Nauk, Ser. Fiz.*, **57**, (2), 165 (1993) [*Bull. Russ. Acad. Sci. Phys.*, **57**, 350 (1993)].
8. Ivanov A.A. *Opt. Spektrosk.*, **80**, 362 (1996) [*Opt. Spectrosc.*, **80**, 318 (1996)].
9. Mikheev G.M., Mogileva T.N. *Kvantovaya Elektron.*, **23**, 943 (1996) [*Quantum Electron.*, **26**, 919 (1996)].
10. Dzhidzhoev M.S., Magnitskii S.A., Saltiel S.M., Tarasevich A.P., Tunkin V.G., Kholodnukh A.I. *Kvantovaya Elektron.*, **8**, 1136 (1981) [*Sov. J. Quantum Electron.*, **11**, 681 (1981)].
11. Tunkin V.G. *Doctoral Thesis* (Moscow: Moscow State University, 1995).
12. Venkin G.V., Kulyuk L.L., Maleev D.I. *Kvantovaya Elektron.*, **3**, 928 (1976) [*Sov. J. Quantum Electron.*, **6**, 504 (1976)].

13. May A.D., Degen V., Stryland J.C., Welsh U.L. *Can. J. Phys.*, **39**, 1769 (1961).
14. Murray J.R., Javan A. *J. Mol. Spectr.*, **29**, 502 (1969).
15. Forsman J.W., Bonamy J., Robert D., Berger J.Ph., Saint-Loup R., Berger H. *Phys. Rev.*, **52**, 2652 (1995).
16. Rautian S.G., Sobel'man I.I. *Usp. Fiz. Nauk*, **90**, 209 (1966).
17. Owyoung A. *Opt. Lett.*, **2** (4), 91 (1983).
18. Murray J.R., Javan A. *J. Mol. Spectr.*, **42**, 1 (1972).
19. Toich A.M., Melton D.W., Roh W.B. *Opt. Commun.*, **55**, 406 (1985).
20. Rahn L.A., Farrow R.L., Rosasco G.J. *Phys. Rev. A*, **43**, 6075 (1991).
21. Cooper V.G., May A.D., Hara E.H., Knapp H.F.P. *Can. J. Phys.*, **46**, 2019 (1968).
22. Konovalov I.G., Morozov V.B., Tunkin V.G., Mikheev V.G. *J. Molec. Structure*, **348**, 41 (1995).
23. Magnitskii S.A. *Candidate Thesis* (Moscow: Moscow State University, 1983).
24. Cooper V.G., May A.D., Gupta B.K. *Can. J. Phys.*, **48**, 725 (1970).
25. Edwards H.G.M., Long D.A., Sherwood G. *J. Raman Spectr.*, **22**, 607 (1991).
26. Berger J.Ph., Saint-Loup R., Berger H., Bonamy J., Robert D. *Phys. Rev.*, **49**, 3396 (1994).
27. Forsman J.W., Bonamy J., Robert D., Berger J.Ph., Saint-Loup R., Berger H. *Phys. Rev.*, **52**, 2652 (1995).
28. Sinclair P.M., Berger J.Ph., Michaut X., Saint-Loup R., Chaux R., Berger H. *Phys. Rev. A*, **54**, 402 (1996).
29. Galatry L. *Phys. Rev. A*, **122**, 1218 (1961).
30. Suetin P.E., Shchegolov G.T., Klestov R.A. *Zh. Tekh. Fiz.*, **29**, 1058 (1959).
31. Mikheev G.M., Maleev D.I., Mogileva T.N. *Kvantovaya Elektron.*, **19**, 45 (1992) [*Sov. J. Quantum Electron.*, **22**, 37 (1992)].